A THESIS

On

CHARACTERIZATION OF SELENIUM NANOSTRUCTURES SYNTHESIZED BY AEROBIC MICROBIAL ROUTE

Submitted in the partial fulfilment of requirement for the award of the

Degree of

Master of Science

In

PHYSICS

Submitted by

Kashika Goyal

(300804011)

Under the Guidance of

Ms. Loveleen Kaur Brar

&

Dr. N. Tejo Prakash

School of Physics and Material Science

THAPAR UNIVERSITY

PATIALA – 147004

INDIA

July 2010

Dedicated

To

My loving Parents

DECLARATION

I hereby declare that thesis entitled **"Characterization of selenium nanostructures Synthesized by Aerobic Microbial route"** in partial fulfilment for the award of the degree of Master of Science in Physics in Thapar University, Patiala is the original work carried out by me under the supervision of **Ms. Loveleen Kaur Brar.** The matter embodied in this thesis has not been submitted anywhere else for the award of any other degree.

Kashika Goyal

Kashika Goyal
M.Sc. (Physics)

Place: **PATIALA**

CERTIFICATE

This is to certify that the thesis entitled **"Characterization of selenium nanostructures synthesized by the Aerobic Microbial route"** submitted by **Kashika Goyal,** Roll No. 300804011, student of M.Sc. (Physics), Thapar University, Patiala, was carried out by her under supervision of **Ms. Loveleen Kaur Brar**. She has not submitted this material for credit towards any other degree at Thapar University, Patiala or at any other University.

Supervisor

Loveleen Kaur Brar 15/7/10

Ms. Loveleen Kaur Brar

Assistant Professor

School of Physics and Material Science

Thapar University, Patiala

N. Tejo Prakash 15/7/10

Dr. N. Tejo Prakash

Assistant Professor

Department of Biotech. & Env. Science

Thapar University, Patiala

Countersigned by:

Dr. O. P. Pandey

Professor and Head

School of Physics and Material Science

Thapar University, Patiala

Dr. R. K. Sharma 20/7/1

Dean of Academic affairs

Thapar University, Patiala

ACKNOWLEDGEMENT

This piece of work will never have been accomplished without our God Almighty with his blessings and his power that work within me and also without the people behind my life for inspiring, guiding, accompanying me through thick and thin.

It is difficult to enunciate in words the deep sense of gratitude which I have for my esteemed supervisor **Ms. Loveleen Kaur Brar**, Assistant Professor, School of Physics and Material Science, Thapar University, Patiala, for her support and patience, motivation, her invaluable assistance and precious guidance helped me in executing this task from its conception to completion.

I take this opportunity to thank **Dr. N. Tejo Prakash**, Assistant Professor, Department of Biotechnology and Environmental Science, Thapar University, Patiala for being my supervisor, and for giving his critical and timely suggestions and immense encouragement throughout my work.

I thank **Dr. K. K. Raina**, Professor and Deputy Director, **Dr. O. P. Pandey**, Professor and Head, SPMS, Thapar University, Patiala, for allowing me to use their lab facilities and always been a source of inspiration for me throughout this work.

I also thank to **Mr. Sumit**, Research Scholar for his timely help and for providing me the samples throughout my work. I also like to thank **Mr. Ravi Shukla**, Research Scholar,for his guidance, cooperation in carrying out experiments. I would also like to thank **Mr. Purushottam Singh**, for his immense patience, for helping and providing data for the experimental work. My sincere thank to all the faculty and staff members of School of Physics and Material Science for their support and encouragement.

Last but not the least I would like to thank my parents for giving me moral support and encouraging me to work hard, without their cooperation this could not have been possible.

Great thanks to all my well wishers

Kashika Goyal

ABSTRACT

Selenium is a non-metallic chemical element, and exhibits many properties like relatively high photoconductivity, high piezoelectric, thermoelectric, and non linear optical responses especially in nanocrystalline form. Selenium nanostructures have been synthesized by aerobic microbial manufacture process. The Se nanostructures produced by the microbe are amorphous, nearly spherical and held together in clusters by a protein coating. The thermal and structural properties of these nanostructures have been studied. Thermal properties of these nanostructures have been studied by DTA and TGA thermograms. Removal of the protein coating by washing with acetone results in growth of crystalline nanostructures. Another method for inducing crystallization is temperature. Heating to ~100 ^{0}C results in the formation of crystalline phase. The nanostructure morphology stays the same. The crystalline phase formed in both the routes is hexagonal and the unit cell dimensions are: a = 4.462 A^0, c = 4.980 A^0. These results imply that the Se nanostructures produced by the microbe are actually clusters of Se atoms held together in a metastable state by a protein coat. This metastable state can be destroyed either by removing the protein coating or by heat treatment which retains the protein coat and hence the shape, but provides enough energy to the atoms within the cluster to crystallize.

LIST OF CONTENTS

List of Figures:

List of Tables:

CHAPTER 1

Introduction

1.1 Selenium

Selenium (Se) is an essential micronutrient in all known forms of life. The word "selenium" has been derived from a Greek word "selene" which mean "moon". It was discovered by Jons Jacob Berzilius [1]. It is a non metallic element of the group 16th (period 4th) of the periodic table. In chemical activity and physical properties it resembles sulphur and tellurium as it lies in between them. It is distributed widely in nature in most rocks and soils. In nature, it occurs usually combined with sulphide or with silver, copper, lead and nickel minerals. It has minimum of 29 isotopes, out of which 5 are stable and are nuclear isomers [1].

1.1.1 Appearance and characteristics:

Selenium exists in several allotropic forms. Three are generally recognised. It can be prepared with either an amorphous or crystalline structure. The colour of amorphous selenium is either red, in powder form, or black, in vitreous form. Crystalline monoclinic selenium is a deep red; crystalline hexagonal selenium, the most stable variety, is a metallic gray (trigonal form) which is composed of long helical chains of selenium atoms. The conductivity of this form is light sensitivity due to which it conducts electricity better in the light than in the dark (photoconductive) and it can convert light directly into electricity (photovoltaic) [2, 3].

1.1.2 Properties of selenium [4, 5]

Atomic Structure of Se:

- Atomic radius: 1.22 A^0
- Atomic volume: 16.45 cm^3/ mol
- Covalent radius: 1.16 A^0
- Crystal structure: hexagonal

- Ionic radius: 0.5 A^0
- Oxidation states: ±2,4,6
- Electronic configuration: $1s^2 2s^2 p^6\ 3s^2 p^6 d^{10}\ 4s^2 p^4$
- Electrons per energy level: 2,8,18,6
- Valence electrons: $4s^2 p^6$

Shell Model:

Chemical Properties:

- Electrochemical equivalent: 0.7365g/amp-hr
- Electron work function: 5.9eV
- Electronegativity: 2.55(pauling)
- Polarizability volume: 3.8 A^{03}
- Heat of fusion: 6.694 kJ/mol
- Ionization potential

  First: 9.752

  Second: 21.19

  Third: 30.82

- Valence electron potential (eV): 120

Physical Properties:

- Atomic mass average: 78.96 amu
- Boiling point: 685 ^{0}C
- Thermal Conductivity: 0.0204 W/cmK
- Density: 4.79 g/cc at 300 K
- Melting point: 221 ^{0}C
- Physical state (at 20 ^{0}C & 1atm): solid
- Specific heat: 0.32 J/gK

Elastic Properties:

- Elastic modulus:

  Bulk: 8.3/GPa

  Rigidity: 3.7/GPa

  Youngs: 58/GPa

Electrical Properties:

- Electrical resistivity: high (10^{-8} Ω m)

Optical Properties:

- Refractive index: 1.000895
- Reflectivity: no data

Typical Reactions:

- Reaction with air : vigorous w/ht ⇒ SeO_2
- Reaction with 15 M HNO_3: mild, H_2SeO_3 , NOX
- Reaction with 6 M HCl: none

1.1.3 Applications of selenium

Non-biologic applications: Elemental selenium is extensively used in variety of industrial and commercial applications. In electronic application selenium is used in photocopying, photocells, light meters and solar cells because of its photovoltaic and photoconductive

properties. Chemically selenium is a catalyst in many chemical reactions and is widely used in synthesis of various laboratory and industrial chemicals. The largest use of selenium is in glass and ceramic manufacturing, where it is used to give a red color to glasses, enamels and glazes as well as to remove color from glass by counteracting the green colour imparted by ferrous impurities.

Biologic applications: Selenium is of importance in biological systems because of its ability to substitute for sulfur in both organic and inorganic molecules, arising from similar ionic radii for the two elements. Selenium analogues of sulfur compounds do not necessarily behave in the same manner in biological systems, with key differences including ease of reduction of their oxyanions and acid strengths of their hydrides. In biological systems, selenium is ultimately reduced to selenide, while sulfur is oxidized to sulfate for excretion. In medical use, the substance loosely called selenium sulfide is the active ingredient in some anti-dandruff shampoos. The selenium compound kills the scalp fungus *Malassezia*, which causes shedding of dry skin fragments. It is also widely used for nutrition in vitamin preparation and other dietary supplements, in small doses (typically 50 to 200 micrograms per day for adult humans) [6].

1.2 Nanotechnology

The word "Nano" means dwarf in Greek language. Use it as a prefix for any unit like a second or a meter and it means a billionth of that unit.

$$1\text{nm} = 10^{-9}\,\text{m}$$

Nanotechnology is defined as a technology where dimensions and tolerances in the range of 0.1 – 100 nm play a critical role [7]. Nanotechnology is very diverse, ranging from extensions of conventional device physics to completely new approaches based upon molecular self assembly, from developing new materials with dimensions on the nanoscale to investigating whether we can directly control matter on the atomic scale [6].

One nanometer is generally considered a magical point on the scale. This is so because there is a sudden shift in all the properties of a material when it just enters into the nanoscale (<100 nm). The reason for this change is the sudden emergence of the some of the basic interactions among the atoms that are averaged out of existence in the bulk material [7]. Another way of explaining the change in properties is to take into consideration the increase in surface area (and hence the surface energy) to volume ratio as we go to smaller particle sizes. The greater the surface for the same volume, the greater is the reactivity. The physical

and chemical reactivity of the element changes at nanoscale due to increase in surface area. Nanoscale structures may possess change in physical properties like band gap, melting point etc [8-10].

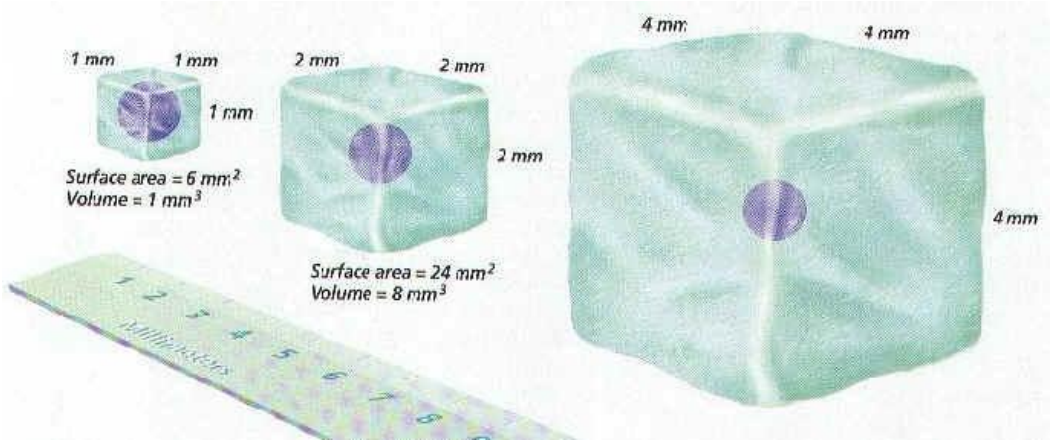

Fig. 1.1 Illustration of increase in surface area to volume ratio [11]

1.3 Selenium nanoparticles

Selenium nanoparticles exhibit many properties like relatively low melting point, high photoconductivity, catalytic activity towards hydration and oxidation reactions, and high piezoelectric, thermoelectric, and non linear optical responses. It also has been of great importance in commercial applications that range from Xerox machines to electrical rectifiers. Amorphous selenium nanoparticles demonstrate not only unique photoelectric, semiconducting and X-ray sensing properties, but also biological activity and good adsorptive ability due to interaction between the nanoparticles and NH, C=O, COO, and C-N groups of the proteins so they may be used as new carriers of constitution of redox enzymes based biosensors. So it is expected that the availability of selenium nanostructures and low-dimensionalities will introduce new applications as a result of size confinement.

Also as we know CdSe is an important semiconducting material with unique optical and electronic properties, which makes them a promising material in the field of opto-electronic devices, biosensors etc. So after studying selenium nanoparticles we will be able to make CdSe nanoparticles. Some of the methods are we can make CdSe nanospheres by direct chemical reaction process of an alkaline selenium solution with an aqueous solution of CdSe complex [12] or CdSe nanocrystals in solution can be made by following synthetic chemical methods including co-dissolvation of dimethylcadmium $Cd(CH_3)_2$ and Se powder in a tri-

alkyl phosphine (–butyl or –octyl) and subsequent injection of the solution into hot coordinating solvent trioctyl phosphine oxide (TOPO) [13].

1.4 Routes for the synthesis of nanostructures

There are different routes for synthesizing nanostructures which are mainly categorized into chemical routes and biological routes.

1.4.1 Chemical routes for the synthesis of Se nanostructures:

These are mainly wet chemical techniques like: [14-17]

- Microemulsion
- Solvent – extraction reduction
- Chemical oxidation/reduction
- Sol-gel
- Coprecipitation
- Hydrothermal / solvothermal
- UV-irradiation
- Template-assisted

1.4.2 Biological synthesis of Se-nanostructures

Synthesis of metal nanoparticles using biological systems has been in vogue in recent past with substantial evidence proving superiority over chemical route. However, the synthesis has been restricted to silver [18], gold [19], palladium and cadmium sulphide materials. There are limited and scarce studies on nano-chalcogenide synthesis especially in the case of selenium. With the growing importance of selenium and selenide containing nanomaterials both in health and engineering applications, the cost-effective route of nanomaterial synthesis using selenium tolerant microbes becomes more so important. The formation of nanoparticles by this method is extremely rapid, requires no toxic chemicals and the nanoparticles are stable for several months. [20, 21, 22, 23]

In this thesis we have continued the work of Tejo Prakash et.al [22]. In this work the bacteria was grown in Se^{2+} ion rich media. Slowly over few days the culture turned red. Closer inspection of bacteria by an environmental scanning electron microscope (E-SEM) having a GSE detector at 0.4-0.7, reveals clusters of nanoparticles on bacterial surface. Energy dispersive X-ray spectroscopy (EDX) gave the information that nanoparticles formed were

essentially of selenium. X-ray diffractometer (XRD) shows that the nanoparticles formed are amorphous in nature. When washed with ethanol we get nano-rosettes of selenium which are crystalline in nature known after characterization by SEM, EDX.

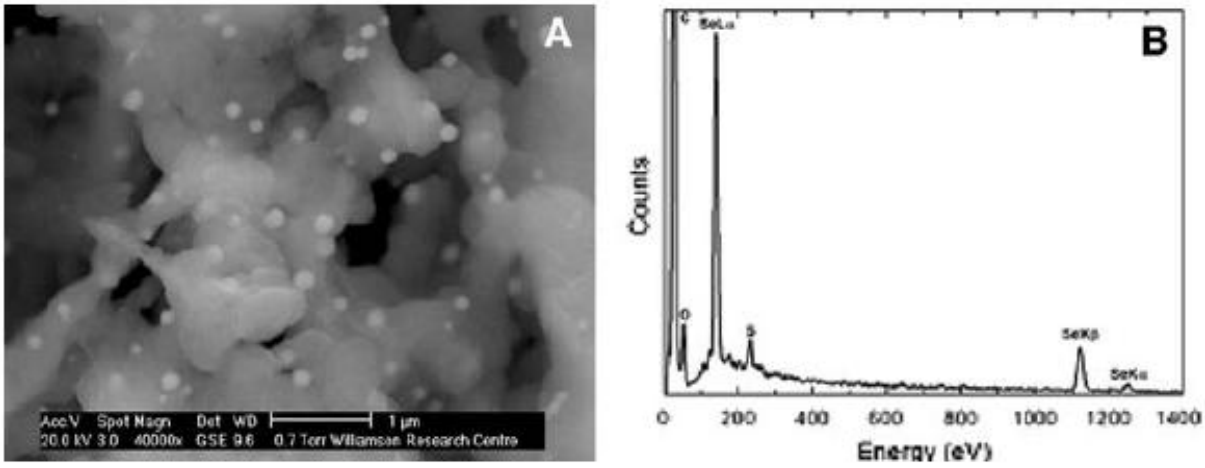

Fig. 1.2 ESEM image (-2 µm) (a) and EDX (b) of selenium nanospheres associated with the Bacillus sp. Biomass

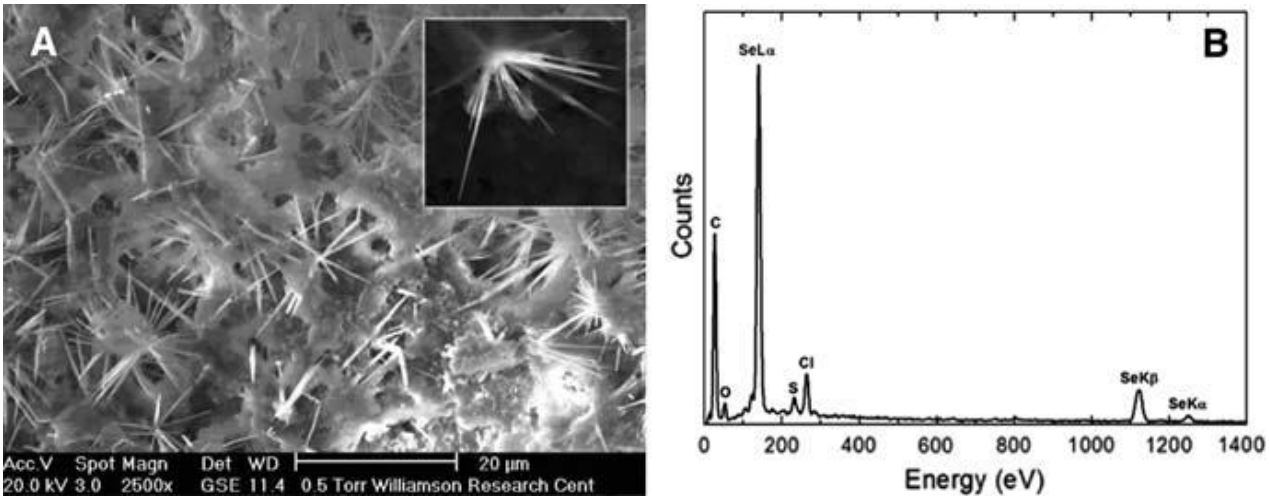

Fig. 1.3 ESEM image (-20µm) (a) and EDX (b) of nanowire/rods formed on biomass in the form of rosettes. Inset shows a closer view of a rosette on 5µm scale.

1.5 Organisation of Thesis

The organisation of the thesis is as follows:

Chapter 1 provides the introduction to the basic properties of selenium and nanoparticles.

Chapter 2 provides the details of the experimental techniques to be used for the characterization of nanostructures.

Chapter 3 provides the details about the methods by which our samples are prepared.

Chapter 4 provides the detailed structural, thermal analysis which we have done.

Chapter 5 provides the conclusion for the thesis and the scope for future work.

Chapter 6 provides the references used in the Thesis

CHAPTER 2

Experimental Techniques

2.1 Structural Characterization

Structural characterization of nanoparticles includes the determination of their morphology, size and crystallinity. In the present study structural characterization of selenium nanostructures is done by X-ray diffraction technique (XRD), optical microscopy, Scanning electron microscopy (SEM), Transmission electron microscopy (TEM).

2.1.1 X-Ray Diffraction Technique (XRD):

X-ray diffraction technique is based on the constructive interference of monochromatic X-rays reflected from a crystalline sample. A collimated beam of X-rays, with a wavelength of the order of the spacing between the scattering centres (atoms in the crystal), is made incident on a specimen and gets diffracted by the crystalline phases in the specimen as shown in Fig 2.1.

Acc. to Bragg's law:

$$n\lambda = 2d \sin\theta$$

Where,

λ is the wavelength of the X-rays

θ is the angle between the incident rays and the surface of the crystal

d is the spacing between layers of atoms

And the constructive interference occurs when n is an integer (whole number) [24]

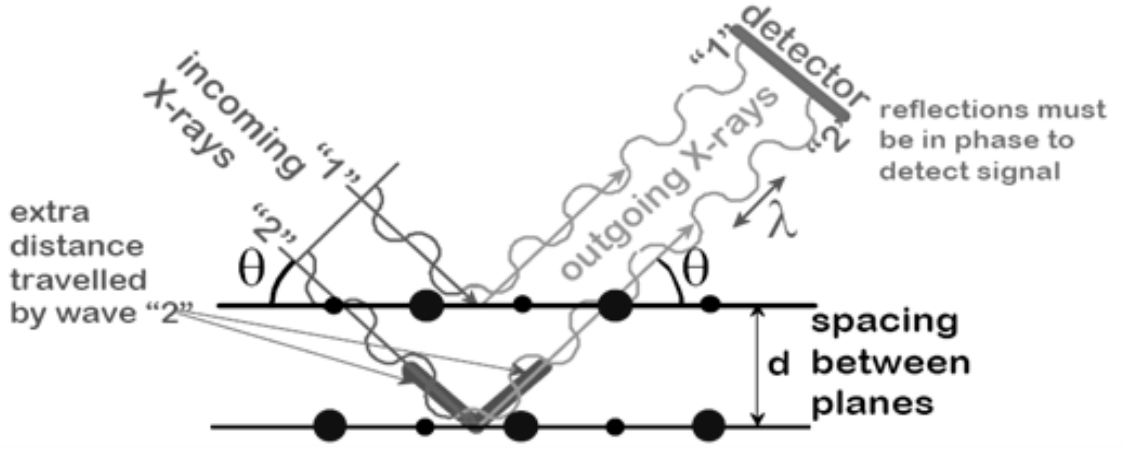

Fig. 2.1 Schematic of Bragg's law

The diffracted X-rays are then detected and counted. The most important component of any difraction technique is the angle between the incident and the diffracted rays.[24]

Conversion of the diffraction peaks to d-spacings (using the above equation) allows the identification of the sample because each sample has a set of unique d-spacings.

X-Ray Powder Diffraction:

X-ray powder diffraction (XRPD) is a non-destructive technique widely applied for the characterisation of crystalline materials. By scanning the sample through a range of 2θ angles, all possible diffraction directions of the lattice are attained due to random orientation of the powdered material.

Sample preparation requirements for XRPD: [25]

- A flat plate sample for XRPD should have a smooth flat surface
  - If the surface is not smooth and flat, X-ray absorption may reduce the intensity of low angle peaks.
  - Parallel-beam optics can be used to analyze samples with odd shapes or rough surfaces.
- Densely packed
- Randomly oriented grains/crystallites
- Grain size less than 10 microns
- 'Infinitely' thick

Information Obtained*:*

This method is used traditionally for phase identification, quantitative analysis and the determination of structure imperfections. It has also been used for the determination of crystal structures and the extraction of three dimensional microstructural properties. [26].

Phase identification using XRD:

Each crystalline solids, produces a distinctive diffraction pattern. Phase identification involves conversion of observed data into intrerplanar spacing, d and relative intensities, I. This data is then compared with the standard database (e.g. JCPDF database) and the phase of the crystal is identified [24].

Particle size analysis:

When the size of the individual crystals is less than about 1μm, the particle becomes important. And the crystals in this size range cause broadening of the XRD lines, the extent of broadening being given by Debye Scherrer formula as

$$T = \frac{0.9\,\lambda}{\beta\ Cos\ \theta_B} \qquad \ldots\ldots\ldots\ldots\ldots\ldots (1)$$

Where,

β = broadening of diffraction line measured at half its maximum intensity (radians)

T = diameter of crystal particle

λ = wavelength of the X-rays

All diffraction lines have a measurable breadth, even when the crystal size exceeds 1000 A^0, due to divergence of the incident beam and size of the sample (in Debye cameras) and width of the source, etc..

The main problem in determining particle size from line breadths is to determine β from the measured breadth β_M of the diffraction line. For this we use Warren's method. Let β_S be the measured breadth, at half-maximum intensity, of the line from the standard. Then β can be find out by

$$\beta^2 = \beta^2_M - \beta^2_S \qquad \ldots\ldots\ldots\ldots\ldots\ldots (2)$$

β obtained from eq.2, can be inserted into eq.1 to yield the particle size T. [27]

Lattice constant/unit cell determination:

Once the crystal structure of the sample is known then the d spacing values obtained from the XRD data can be used to determine the lattice constant.

Selenium in our system exhibits hexagonal crystal structure [22]. For hexagonal crystal structure a = b ≠ c and α = β = 90^0, γ = 120^0. Fig 2.2 shows the hexagonal crystal structure [28]

Formula for finding the lattice parameters of the hexagonal crystal structure is [27]:

$$\frac{1}{d^2} = \frac{4}{3}\left(\frac{h^2 + hk + k^2}{a^2}\right) + \frac{l^2}{c^2} = \frac{4\sin^2\theta}{\lambda^2}$$

Where,

d is the intrerplanar spacing

h, k, l are the miller indices

a, c are the lattice parameters

λ is the characteristic wavelength

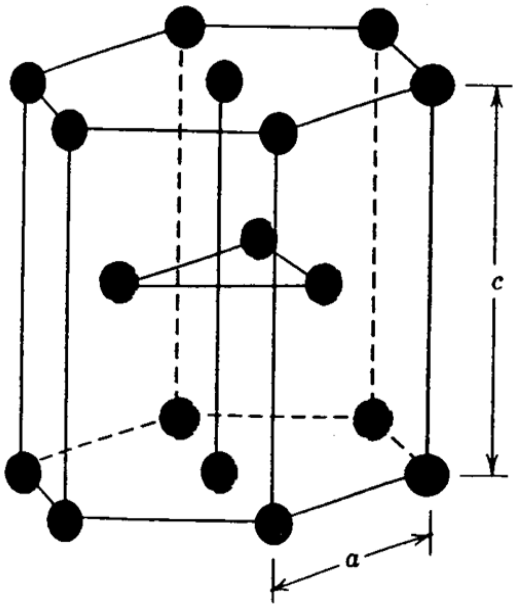

Fig. 2.2 Hexagonal crystal structure of selenium [28]

2.1.2 Optical Microscopy

Optical microscopy is the oldest and most utilized method for microstructural characterization of materials. It uses the geometry and refractive indices of transparent optical components (lenses) to focus light and form a magnified image [29].

Basic requirement for an optical microscope is the ability to resolve details in the image.

Resolution defines the smallest separation of two points in the object that can be distinctly reproduced in the image.

Magnification is how much bigger we can make something appear.

Contrast is the difference between the brightness of various details in the object, and the difference as compared with the background [30]

Image contrast C is defined as:

$$C = \frac{S_{specimen} - S_{background}}{S_{background}}$$

$S_{specimen}$ and $S_{background}$ are the measured intensities from the specimen and background [31]

Depth of field is the range of position for the object in which our eye cannot detect change in the sharpness of the image [30].

Main components of any light microscope are: [29]

- Transmission source
- Reflection source
- Condenser optics – makes the light rays parallel for even illumination
- Apertures – match the radius of light source to the objective

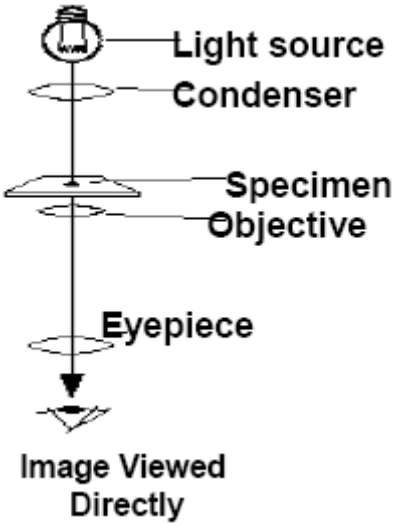

Fig. 2.3 Image formation in Optical Microscope [32]

Why Electron microscopy?

- **Primary reason : spot size**

$$\lambda = \frac{h}{p} = \frac{h}{mv}\sqrt{1 - \frac{v^2}{c^2}}$$

For an electron with KE = 1 eV and rest mass energy 0.511 MeV, the associated DeBroglie wavelength is 1.23 nm, about a thousand times smaller than a 1 eV photon [33].

- **Highest typical resolution** in case of Optical microscope is 200 nm and for Electron microscope is .1 nm, also the electron microscopy has large depth of field, which allows a large amount of sample to be in focus at one time and produces an image that is a good representation of the three- dimensional sample [34].

2.1.3 Scanning Electron Microscopy

The scanning electron microscope (SEM) is an electron microscope which images the sample surface by scanning it with a high-energy beam of electrons in a raster scan pattern. The electrons interact with the atoms of the sample producing signals which contain information about the sample's surface topography, composition and other properties such as electrical conductivity [6]. The SEM is routinely used to generate high-resolution images of morphology of the objects and to show spatial variations in chemical compositions. SEM is also widely used to identify phases based on qualitative chemical analysis and/or crystalline structure. Precise measurement of very small features and objects down to 20 nm in size can be routinely accomplished using the SEM [24].

Properties of the material which are probed by SEM:

- **Topography**
  The surface features of an object or "how it looks", its texture; direct relation between these features and material properties
- **Morphology**
  The shape and size of the particles making up the object; direct relation between these structures and material properties
- **Composition**
  The elements and the compounds that the object is composed of and the relative amounts of them; direct relationship between composition and material properties
- **Crystallographic information**
  How the atoms are arranged in the object; direct relation between these arrangements and material properties [32]

Electron sample interactions:

When an electron beam strikes a sample, a large number of signals are generated as shown in Fig 2.4.

We can divide the signals into two broad categories [32]:

a) Electron signals
b) Photon signals

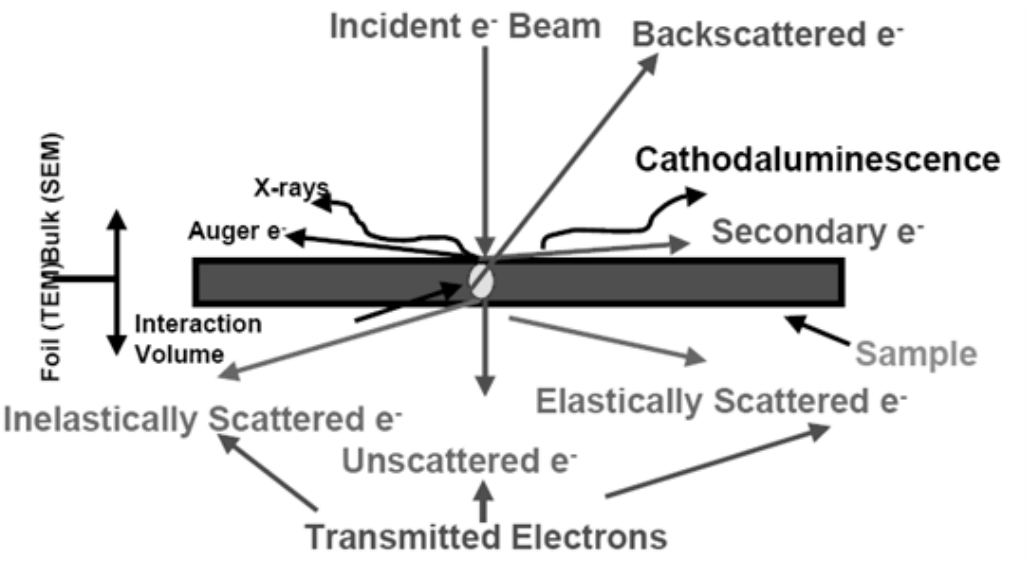

Fig. 2.4 Schematic showing all possible electron-sample interactions

The SEM electron probe is a focused probe of electrons accelerated to moderately high energy ranging from a few hundred eV to 50 KeV and positioned onto the sample by electromagnetic fields. This beam of electrons interacts with atoms in the specimen by a variety of mechanisms when they impinge on a point on the surface of the specimen as shown above [35].

Interaction Volume: The simultaneous loss of energy and change in trajectory produces an interaction volume within the bulk which extends from less than 100 nm to around 5µm into the surface. The size of the interaction volume depends on the electron's landing energy, angle of incidence, the atomic no. of the specimen and the specimen's density.

Sampling volume: The signals resulting from various interactions will have different depths within the sample from which they can escape due to their unique physical properties and energies. This gives rise to sampling volume, from which a given signal escapes the solid and is

a fraction of the interaction volume. The spatial resolution is determined by the sampling volume and the signal distribution within it.

Image appears to be in focus if the sampling volume of the given signal is smaller than the picture element size at the given magnification. This also defines the resolution of SEM. The sampling volume should be smaller than the feature which needs to be resolved [36].

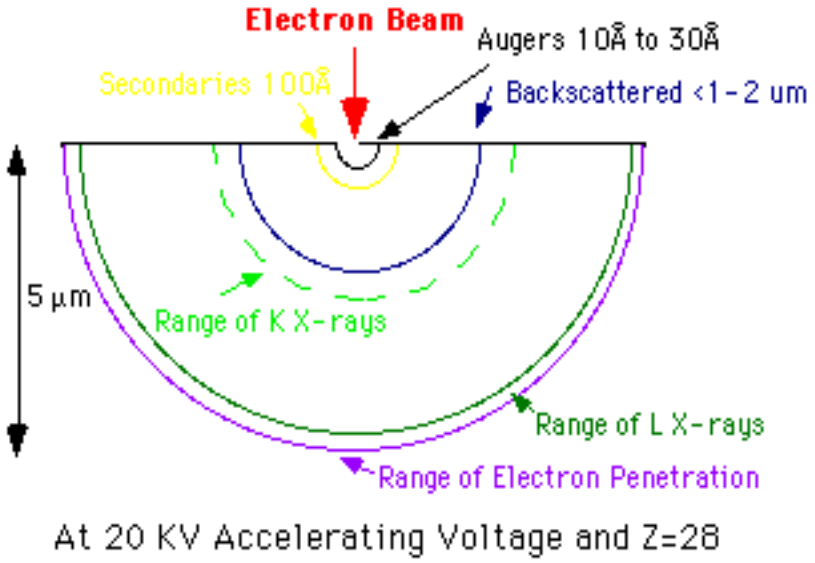

Fig. 2.5 Specimen interaction volume [37]

Depth of field in SEM is 30mm i.e. it has more than 300 times the depth of field of a light microscope. In SEM generally the resolution is 5nm- 20 nm but resolution of 1nm is achievable with field emission electron gun. [32].

Sample preparation requirements for SEM:

- Sample must be of an appropriate size to fit in the specimen chamber.
- For conventional imaging in SEM, specimen must be electrically conductive and electrically grounded to prevent the accumulation of electrostatic charges at surface.
- Nonconductive specimens tend to charge when scanned by the electron beam, and especially in secondary electron imaging mode, this causes scanning faults and other image artifacts. They are therefore usually coated with an ultrathin coating of electrically-conducting material, commonly gold, deposited on the sample either by low vacuum sputter coating or by high vacuum evaporation.

- Nonconducting specimens may be imaged uncoated using specialized SEM instrumentation such as the "Environmental SEM" (ESEM)

2.1.4 Transmission Electron Microscopy

In Transmission electron microscope (TEM) a beam of accelerated (100 KeV or higher (up to 1MeV)) electrons is projected onto a thin specimen (less than 200 nm) by means of the condenser lens system. The electron beam interacts with the specimen as it passes through it. The greatest advantages that TEM offers are the high magnification ranging from 50 to 10^6 and its ability to provide both image and diffraction information from a single sample.

The scattering processes experienced by electrons during their passage through the specimen determine the information obtained. Elastic scattering involves no energy loss and gives rise to diffraction patterns. Inelastic interactions between primary electrons and sample electrons at heterogeneities such as grain boundaries, dislocations, second phase particles, defects, density variations, etc., cause complex absorption and scattering effects, leading to a spatial variation in the intensity of the transmitted electrons [38].

Information TEM gives:

- **Morphology**

  The size, shape and arrangement of the particles which make up the specimen as well as the relationship with each other on the scale of atomic diameters.

- **Crystallographic Information**

  The arrangement of atoms in the specimen and their degree of order, detection of atomic-scale defects in areas a few nanometres in diameter

- **Compositional Information (if so equipped)**

  The elements and compounds the sample is composed of and their relative ratios, in areas a few nanometres in diameter [39]

Modes of imaging: [36]

- **Bright Field Imaging**

  It is an imaging mode in TEM that uses only unscattered electrons to form the image. Contrast in such an image is due entirely to thickness and density variations in a sample.

- **CBED:** *Convergent Beam Electron Diffraction*

  An electron probe is tightly focused on a TEM specimen and the resulting pattern of diffracted electrons is observed. The pattern contains information on the crystal symmetry and atomic and electronic structure of the sample. Regions as small as 0.2 nm may be examine.

- **Dark Field Imaging**

  It uses a single diffracted beam to form the image in a TEM. This causes all regions of the specimen not of the same crystal structure and orientation as the region which produced the diffracted beam to be represented as very dark in the final image; allowing phase differentiation visually in the TEM.

- **Hi-resolution Imaging**

  Direct imaging of the specimen lattice is done in HRTEM. This is accomplished by allowing some of the diffraction image to overlay the bright field image, enhancing the contrast along the lattice lines. It allows direct measurement of lattice parameters, inspection of individual defects and grain orientation.

- **SAED:** *Selected Area Electron Diffraction*

  An aperture is used to define the area from which a diffraction pattern is formed in a TEM specimen. The resulting patterns contain information about phases present (lattice spacing measurement) and sample orientation.

Sample preparation requirements for TEM:

Due to the strong interaction between electrons and matter, the specimens have to be rather thin (<< 1000 nm) for TEM investigation. Thus, bulk materials have to be thinned to make them electron transparent. This is done either by simply crushing them and subsequently depositing some fragments on a carbon foil or by mechanical grinding and ion milling. To observe the longitudinal structure of nanostructures, they are simply dispersed in ethanol, and some droplets are deposited on a holey carbon foil supported on a copper grid.

2.2 Thermal Characterization

Thermal analysis comprises a group of techniques in which a physical property of a substance is measured as a function of temperature, while the substance is subjected to a controlled temperature programme.

Generalized instrument: [40]

Temperature programmer

↓

Sample in furnace with controlled atmosphere

↓ X-axis ↓ y-axis

Temperature property

Output: Plot of the property (y axis) versus T.

2.2.1 Differential Thermal Analysis:

Differential Thermal Analysis (DTA) is technique in which the temperature difference between a substance and a reference material is measured as a function of temperature while the substance and reference material are subjected to the same controlled temperature programme [41]. Fig. 2.6 gives the schematic of DTA.

When the sample undergoes an endothermic or exothermic change ΔT becomes different [40]**.** In the final output the temperature difference (ΔT) is plotted w.r.t. temperature or time on the y-axis increasing from left to right [41].

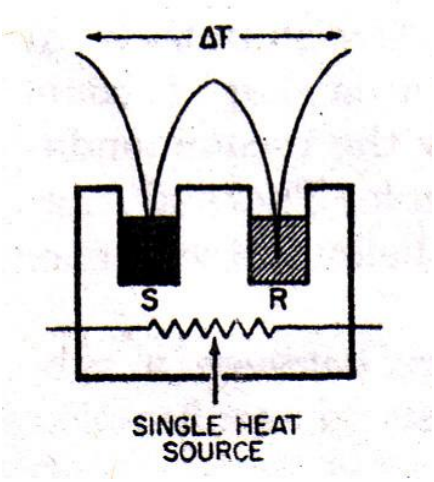

Fig. 2.6 Schematic illustration of DTA set up [36]

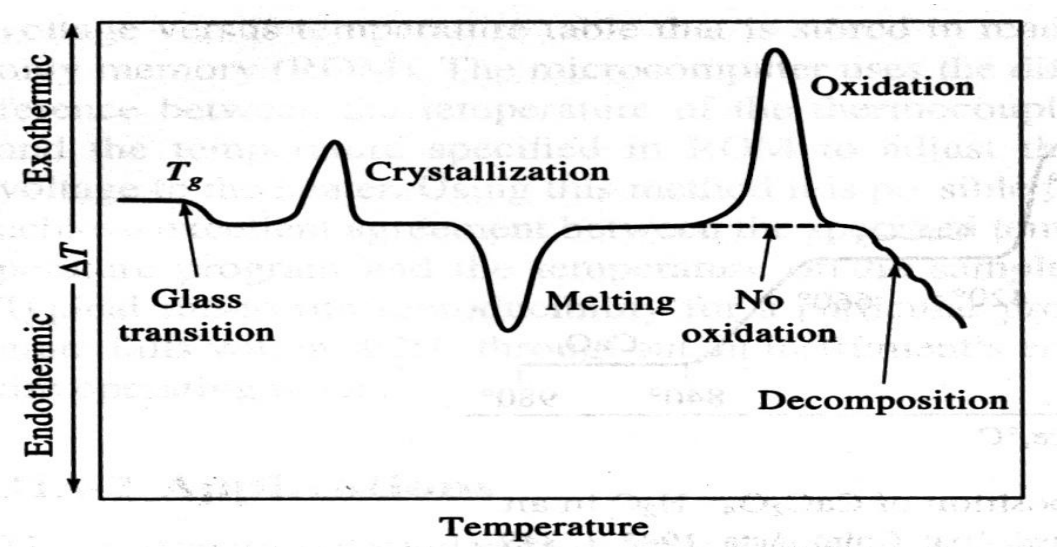

Fig. 2.7 Schematic of all possible transitions in DTA

Fig. 2.7 gives the schematic of all possible transitions in a DTA. So from DTA of a given material following information about the phase-transitions (if any) can be determined:

- The glass transition temperature T_g.
- The point of crystallization.
- The melting point of our sample and also comment on its purity.
- Point of oxidation
- By finding the area under the curve gives the respective heat of fusion and heat of crystallization.
- Percentage of crystallinity for composites

We will discuss in detail the melting and the crystallization curves.

- ## Melting

  Melting is change from solid to liquid state. It is accompanied by an endothermic enthalpy change. Melting curves obtained in DTA depend on the purity and crystallinity of the sample, the thermal resistance, R_0, between the sample pan and the sample holder and the rate of change of temperature for the given programme [36].

Methodology for the determination of melting point: For a given instrument the thermal resistance R_0 is always constant. From the curve of fusion of an ultra pure metal the leading edge of the peak is extrapolated downwards and its intersection with the baseline is defined as the onset temperature (Fig. 2.8).

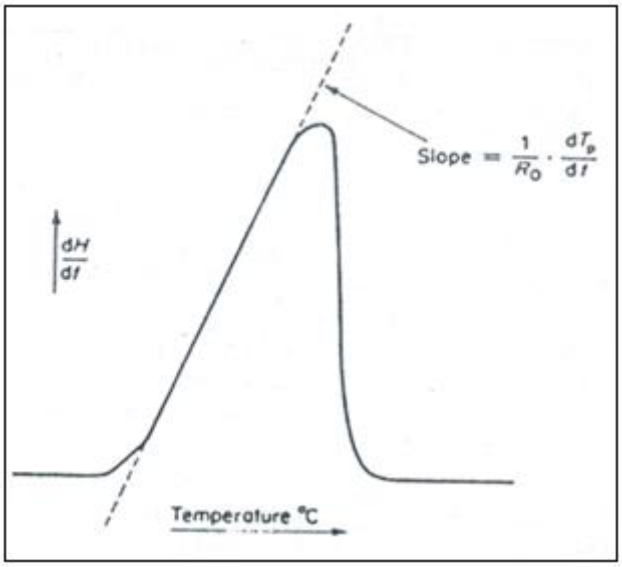

Fig. 2.8 Thermogram for the fusion of 99.99% pure metal

The true melting temperature of any other sample is determined as an extrapolated onset temperature using the slope determined with the ultrapure metal. (Fig. 2.9)

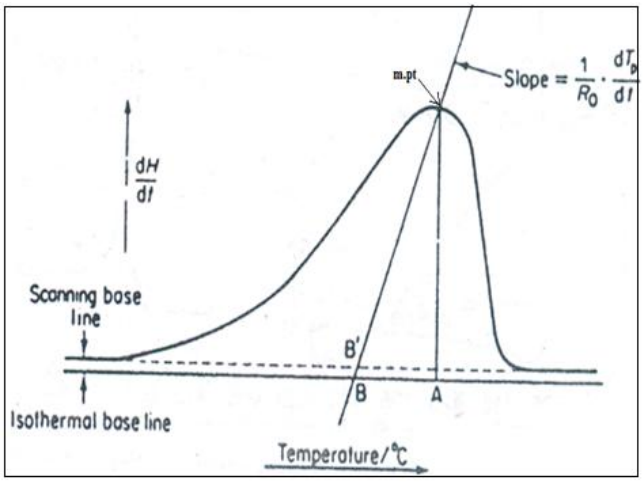

Fig. 2.9 Details of the onset temperature determination for a given sample in DTA

Steps involved:

- Determine the leading edge slope for a standard ultrapure metal at the same heating rate as to be used for the sample
- For the DTA curve of the sample draw the base line.
- Determine the point of intersection with the extrapolated leading edge slope passing through the apex of the curve.

- This is the onset temperature for a given transition and for the melting transitions it is called the melting point.

- **Crystallization**

  The cooling curve crystallisation (exothermic) characterizes the change in enthalpy when a material in the amorphous state is transformed into a solid crystalline state, as the temperature decreases.

The cooling rate determines the position of the crystallisation curve on the temperature scale. As the cooling rate increases, the crystallization curve is displaced toward lower temperatures. Crystallization can be measured not only during cooling but also during heating and is called **cold crystallisation**. It can occur if the material is quenched from the melt without allowing the crystallisation to occur [42] or for the case of protein/organic capping mediated precipitation of a material. Crystallization point can be determined in the same way as the melting point.

2.2.2 Thermo Gravimetric Analysis

Thermo Gravimetric Analysis (TGA) is a simple analytical technique that measures the weight loss (or weight gain) of a material as a function of temperature. As materials are heated, they can lose weight from a simple process such as drying, or from chemical reactions that liberate gasses. Some materials can gain weight by reacting with the atmosphere in the testing environment [43]. In TGA, the change of mass of a specimen is measured either absolutely in milligrams or relatively as a percentage of the starting mass, and plotted against temperature or time. The mass loss/gain can be continuous, single step or multistep.

Single-step change of mass:

Fig. 2.10 below illustrates the characteristic temperatures involved in a single-step loss of mass.

Starting point A: Intersection of extrapolated starting mass with the tangent applied to the maximum slope of the TG curve

End point B: Intersection of extrapolated end mass after reaction with the tangent applied to the maximum slope of the TG curve

Midpoint C: Intersection of the TG curve with the line parallel to the abscissa that is midway between A and B

Starting point temp. /time T_A/t_A: Temperature/time at the start

End point temp. /time T_B/t_B: Temperature/time at the end

Mid point temp. /time T_C/t_C: Temperature/time at the mid point

Starting mass m_S: Mass before heating

End mass m_f: Mass after end temperature attained
[42]

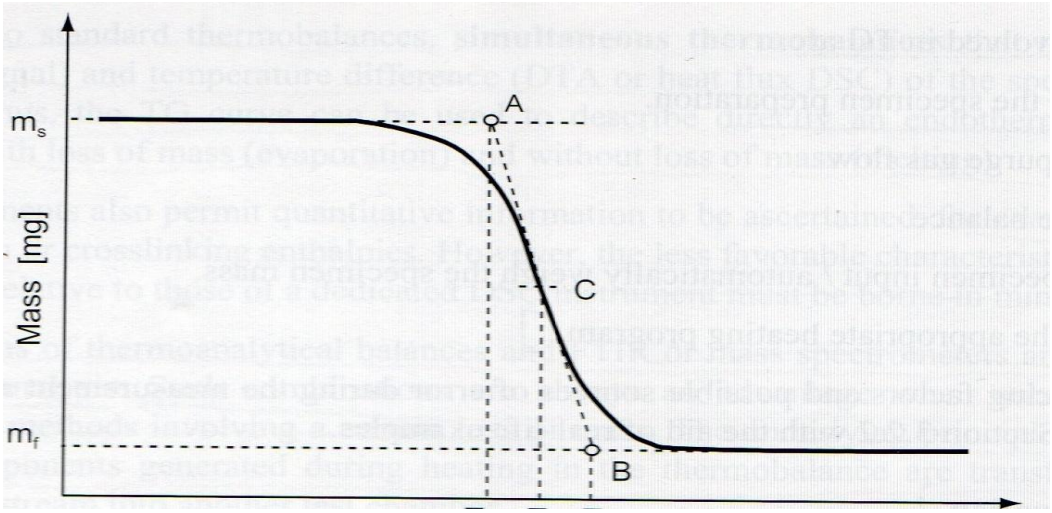

Fig. 2.10 Schematic of transitions in TGA

CHAPTER 3

Sample Preparation

In this work the Se prepared via the biological route has been characterized using various techniques. For comparison we have used commercially available selenium [44] and also the selenium nanoparticles prepared via the chemical route.

3.1 Biological-Selenium nanostructures

Growth and tolerance in Se-spiked medium as well as the selenium uptake studies for the bacteria have been done as per the methods reported earlier [23].

3.1.1 Isolation of Selenium nanostructures from Bacteria:

For the bacterial culture grown in 200 ml TSB media containing 5mM Se^{+4} ions the red bacterial biomass was isolated from the media by centrifugation at 8000 rpm for 10 minutes. The biomass was then washed twice with saline and the washed biomass was resuspended in 2-3 ml distilled water. 0.4 ml of this cell suspension was taken in a round bottom flask and 0.8 ml of saturated KOH solution was added. The round bottom flask was then incubated at 70 ^{0}C in water bath with slow shaking till the solution turned reddish–brown. The solution was centrifuged at 14,000 rpm for 10 minutes. After centrifugation the clear reddish–brown solution was transferred into a clean test tube and 2-3 ml of saturated solution of Ammonium sulphate was added. The mixture was vortexed for 2 minutes and again centrifuged at 14,000 rpm for 10 minutes. After centrifugation the upper clear supernatant was discarded and red pellet was washed twice with d.H_2O and dried at 37 ^{0}C. So we get isolated selenium nanostructures.

3.2 Chemical route for the formation of selenium nanoparticles: [15]

100 mg of Bovine Serum Albumin (BSA) [45] was added to 10 ml of 100 mM sodium selenite (Na_2SeO_3) [46] solution. The solution was then shaken slowly to dissolve BSA [48] and to prevent frothing. After that 100 mg of Ascorbic acid [47] was added to the test tube, and test tube was shaken slowly. Then it was vortexed for 5 minutes and kept at 4 ^{0}C for 1 hour. The red solution obtained was centrifuged at 14,000 rpm for 15 minutes at 4 ^{0}C. After centrifugation the clear supernatant was discarded and the red pellet was washed twice with distilled water. The washed pellet was resuspended into 2 ml distilled water. Then 10 mg of Sodium Dodecyl Sulphate (SDS) [48] was dissolved in upper solution and vortexed for 1 minute, after the addition of SDS, a clear red solution was obtained. Then 100 μl of this

clear solution obtained after addition of SDS was taken into a fresh 2 ml eppondorf, and 1.5 ml of Acetone [49] was added to it and it is kept at 40 ^{0}C for 1 hour. After 1 hour of incubation, red solution turned into black, which was centrifuged at 8000 rpm for 10 minutes. After centrifugation the clear supernatant was discarded and the black pellet was washed twice with distilled water. The black pellet was resuspended into 1ml of distilled water.

3.3 Sample details:

The various samples used in the present study are:

S. No.	Sample name	Detail
1.	Se B	Biologically prepared selenium (with the method mentioned in section 3.1)
2.	Se B1	Biologically prepared selenium washed with acetone
3.	Se B2	Biologically prepared selenium autoclaved at 110 ^{0}C for 15-20 minutes.
4.	Se B3	Biologically prepared selenium autoclaved at 121 ^{0}C for 15-20 minutes.
5.	Se Bulk	Commercial Selenium
6.	Se CS	Chemically prepared selenium
7.	Se CS1	Chemically prepared selenium washed with acetone

Table 3.1 Details of the given sample naming

CHAPTER 4

Results

&

Discussions

4.1 Thermal Analysis

In the present study DTA and TGA curves have been recorded using Perkin Elmer Diamond TG/ DTA. The rate of heating was 10 ^{0}C per minute and Argon is used as the Purge gas. The measured thermal analysis temperature range was 50 ^{0}C to 240 ^{0}C.

4.1.1 Differential Thermal Analysis

Data Analysis:

Fig. 4.1 shows the DTA curve for the fusion of Se B1 sample measured in the temperature range of 50 ^{0}C to 239 ^{0}C. The DTA curve shows only one sharp endothermic peak around the melting temperature of selenium.

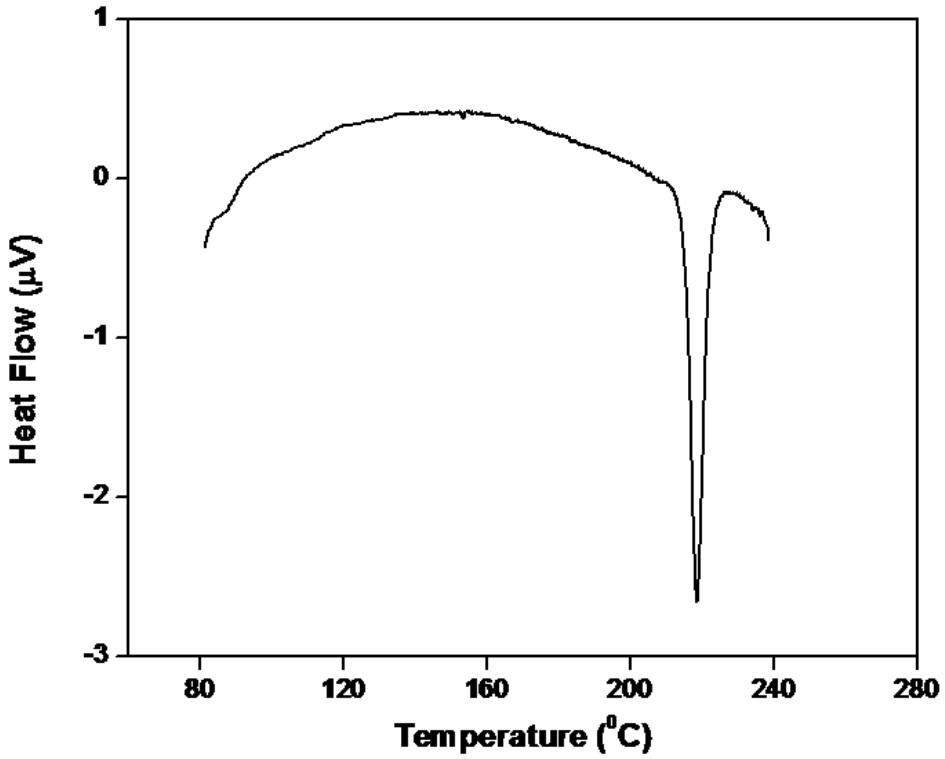

Fig. 4.1 DTA curve for sample SeB1

Using the method mentioned in chapter 2 we have determined the melting point of selenium (Fig. 4.3).

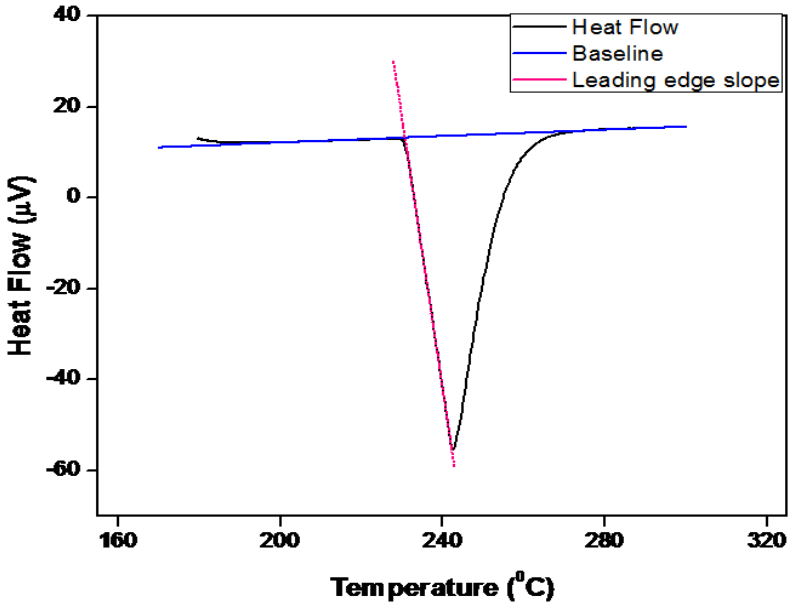

Fig. 4.2 DTA curve for 99.99 % pure tin

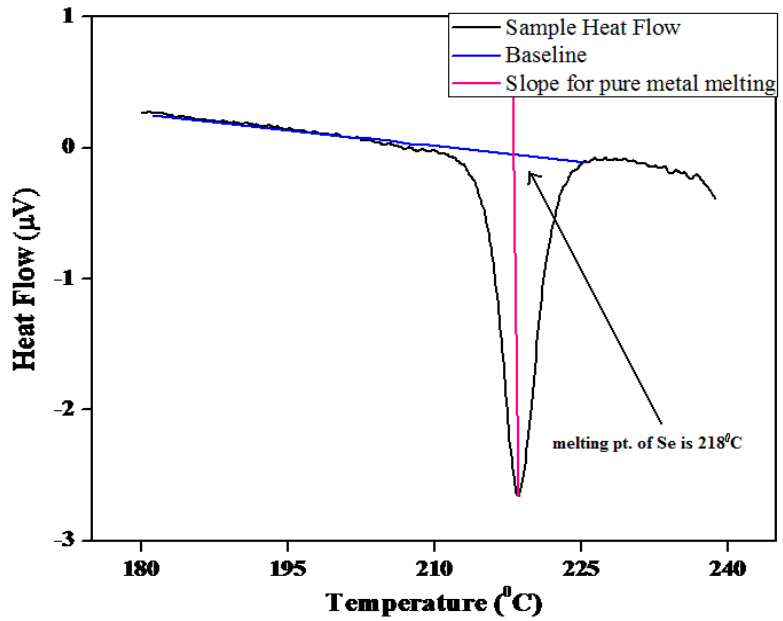

Fig. 4.3 DTA curve showing calculation of melting point for Se B1

Melting point of selenium = 218 ^{0}C

For sample Se B, which is amorphous [22], an exothermic peak is observed (Fig. 4.4). This is peak is much below the melting temperature for selenium. The onset temperature for this transition is determined using the same technique and comes out to be 95.9 ^{0}C

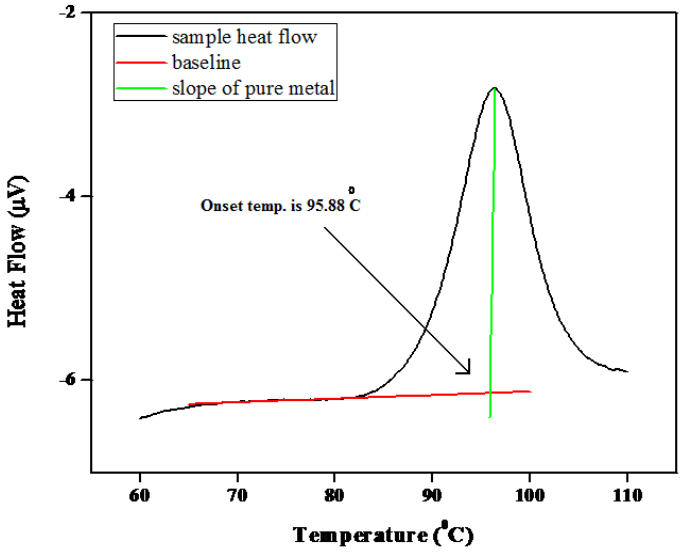

Fig. 4.4 DTA curve showing crystallisation point for the sample Se B

So for the crystalline sample Se B1 [22], only the melting peak is observed whereas for the amorphous sample Se B, an additional exothermic phase transition is observed at ~96 ^{0}C.

4.1.2 Thermo Gravimetric Analysis

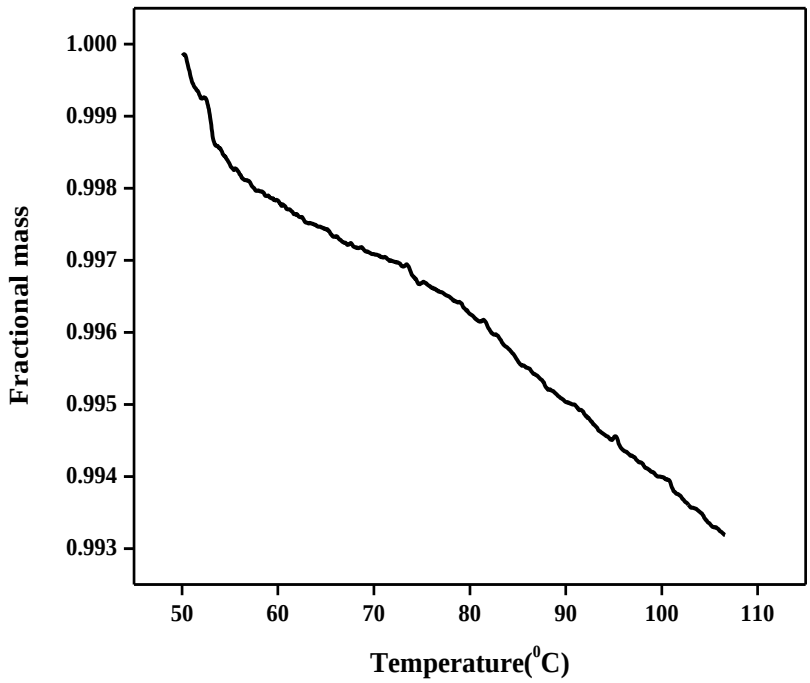

Fig. 4.5 TG curve for the sample Se B.

The TGA curve for the sample Se B in the region of interest is shown in Fig. 4.5. As in this curve for the Se B1 sample also, we observe no mass loss.

4.2 Structural Analysis

4.2.1 X-ray diffraction studies

In the present study, XRD patterns have been recorded using X'PERT PRO analytical powder X-ray diffractometer (Rikagu) using Cu Kα1 as characteristic wavelength which is equal to 1.54060 A^0 and Cu Kα1 radiation is operating at 45kV, 40 mA.

Sample for XRD study is prepared by drying the suspension by lyophilisation. The X-ray diffractometer conditions are set as

Start position [2Theta] - 5.0066^0

End position [2Theta] - 79.9906^0

Step size [2Theta] - 0.0130^0

Scan step time [s] - 18.8700

Fig. 4.6-4.8 are the XRD patterns of different samples.

In our sample the sharp diffraction peaks indicate the good crystallization of the products. Peaks of (100), (101), (110), (012), (200), (201), (003) are clearly observed, and consistent with the values of the hexagonal phase of Se crystal structures (JCPDS file No. 86-2246)

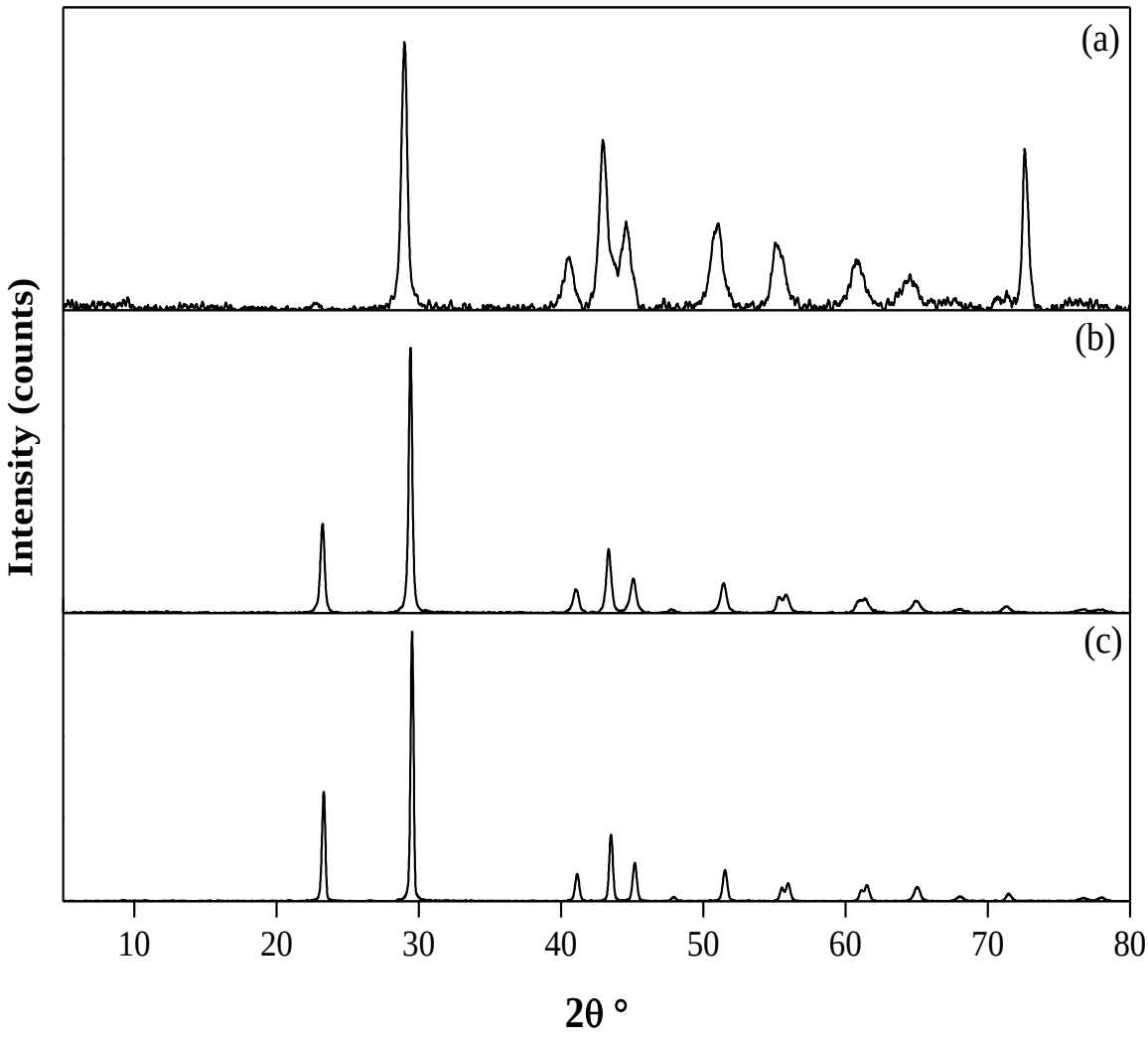

Fig. 4.6 XRD pattern of samples Se B1 (a), Se CS (b), Se Bulk (c)

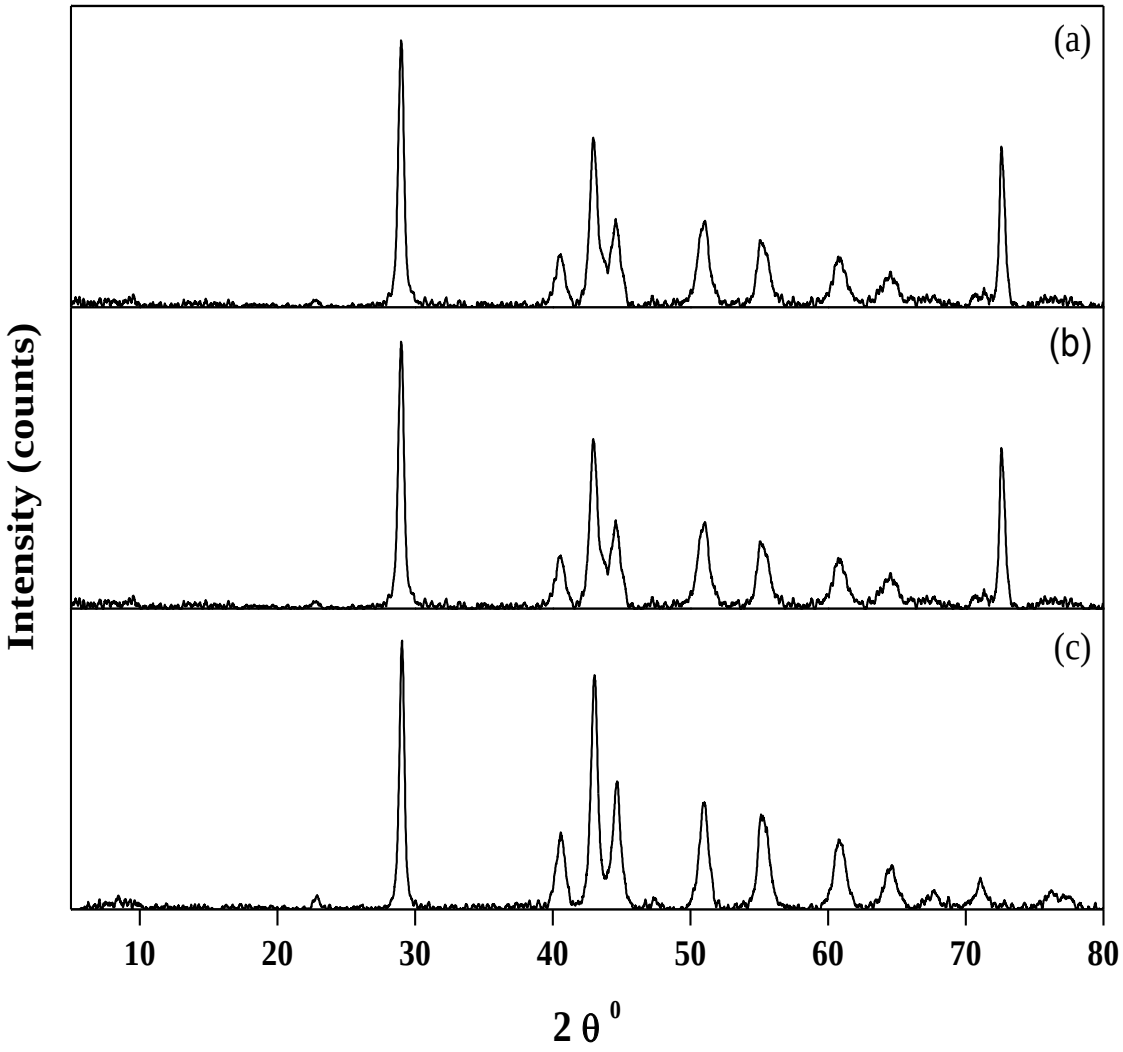

Fig. 4.7 XRD pattern of samples Se B1 (a), Se B2 (b), Se B3 (c)

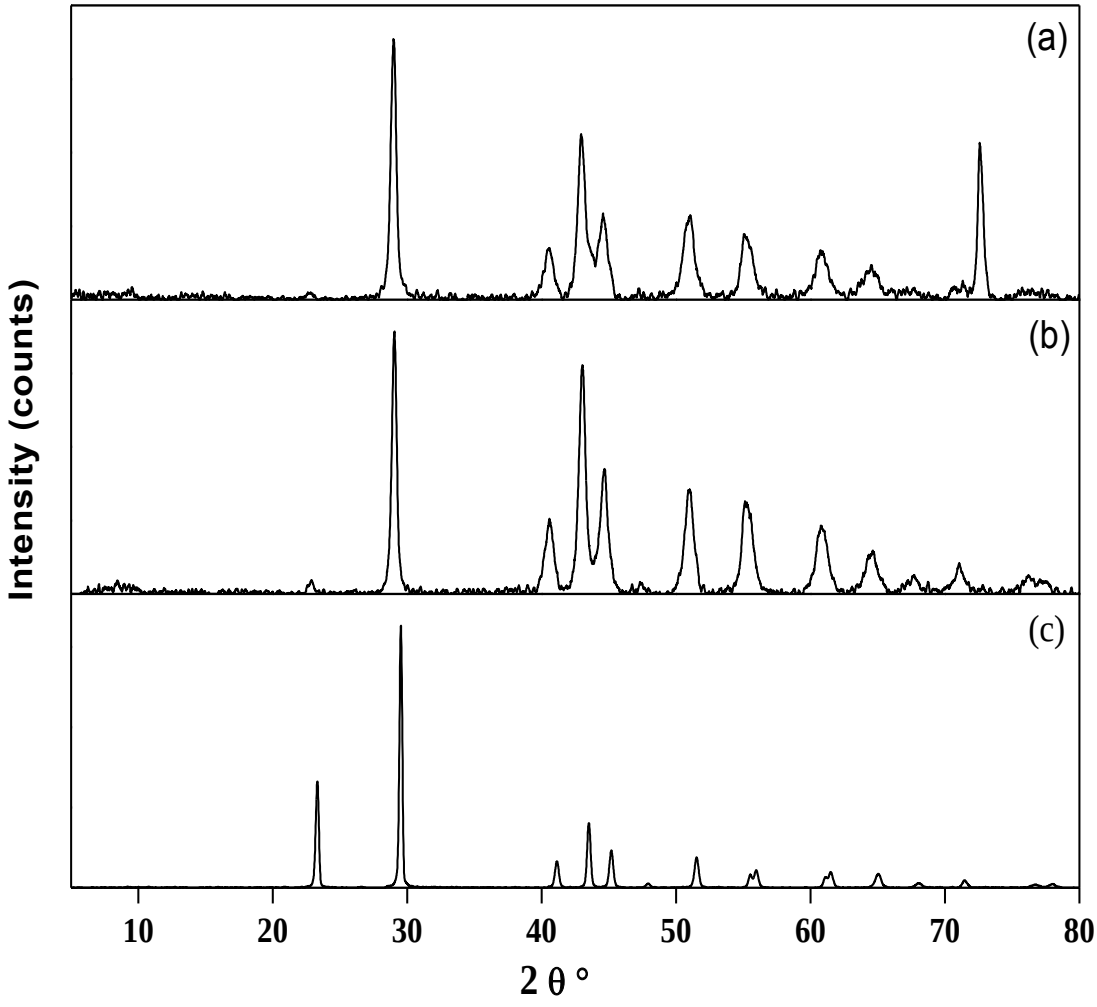

Fig. 4.8 XRD pattern of samples Se B1 (a), Se B2 (b), Se Bulk (c)

XRD data analysis

- The Se B1 shows the similar crystal structure as the commercially available bulk Se and that prepared via the chemical route (Fig. 4.6).
- The crystalline phase observed is the hexagonal phase selenium (JCPDS file No. 86-2246).
- The Se B2 and Se B3 samples show similar crystalline structure as the Se B1 sample (Fig. 4.7).This proves that the exothermic peak observed in DTA is actually the crystallization peak.
- Similar results were also obtained when the Se B sample was dried, heated to 120 ^{0}C in an oven (data not shown).
- The Se B1, Se B2 and Se B3 samples show marked broadening of the XRD peaks confirming that the samples are indeed nanostructures. The size analysis has been done.
- Sample Se B is completely amorphous.
- The crystallinity can be induced in the sample Se B either by removing the protein network by dissolving it in acetone or by heating. In the latter case the protein network though modified would still be intact.

Unit cell determination analysis:

For hexagonal structure we know: [27]

$$\frac{1}{d^2} = \frac{4}{3}\left(\frac{h^2 + hk + k^2}{a^2}\right) + \frac{l^2}{c^2} = \frac{4\sin^2\theta}{\lambda^2}$$

Using above formula we find lattice constants:

a = 4.462 A^0, c = 4.980 A^0

Hence, c / a ratio = 1.116

This is in agreement with the reported values of a and c for selenium [50]

Particle Size analysis:

Average particle size of the nanostructures has been calculated from the recorded XRD pattern using the Debye Scherrer Formula as-

S. No.	Sample name	Average particle size
1.	Se B	Sample is completely amorphous.
2.	Se B1	40.06 nm
3.	Se B2	21.01 nm
4.	Se B3	25.05 nm
5.	Se CS	Sample is partially amorphous.
6.	Se CS 1	51.92 nm
7.	Se CS 2	66.64 nm

Table 4.1 Calculated average particle size of each sample

4.2.2 Imaging

Optical imaging: The optical images were taken with Optical Microscope (OLYMPUS BX51) at 500X magnification. The images were taken in transmission mode and recorded using the CCD camera (OLYMPUS DP 12) attached to the instrument.

Sample Preparation: A drop of the dilute solution (in de-ionized water) of the relevant sample was placed on a clean glass slide and dried.

SEM imaging: In the present study SEM images were taken with Scanning Electron Microscope (JEOL – JSM 6512) operated at 15 kV.

Sample Preparation: A 20 μl drop of the dilute solution (in de-ionized water) of the relevant sample was placed on copper tape and dried under a lamp. The samples were coated with gold before imaging.

TEM imaging: In the present study TEM images are taken with Transmission Electron Microscope (HITACHI 7500) having resolution 2 A^0, operated at 80 kV.

Sample Preparation: A 20 μl drop of the dilute solution (in de-ionized water) of the relevant sample was placed on the carbon coated copper grid. The dried samples/grids were mounted in the microscope without any further steps.

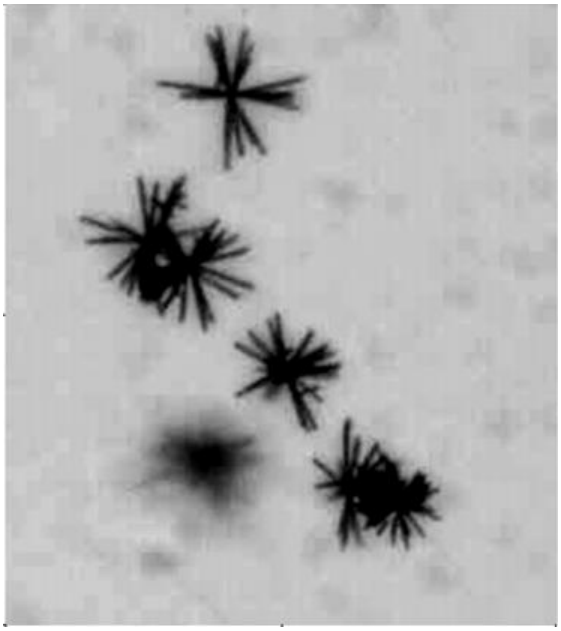

Fig. 4.9 The optical image of the biomass (with the nanostructures intact) after acetone wash

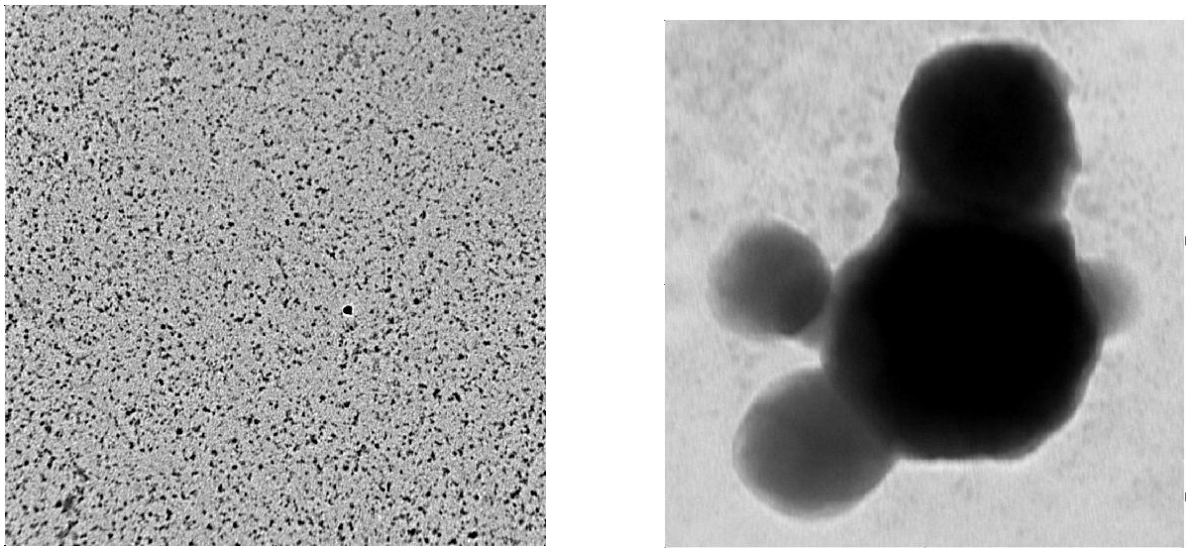

Fig. 4.10 a) 1μm X 1μm b) 150 nm X 150 nm TEM image of the Se B

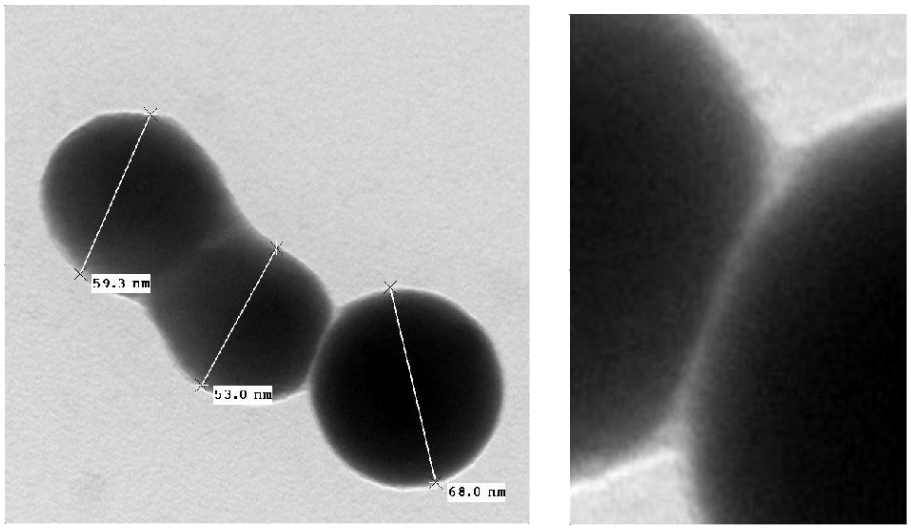

Fig. 4.11 a) 150 nm X 150 nm TEM image of the Se B b) 31 nm X 47nm image showing the details of the protein network holding Selenium nanostructures together in a)

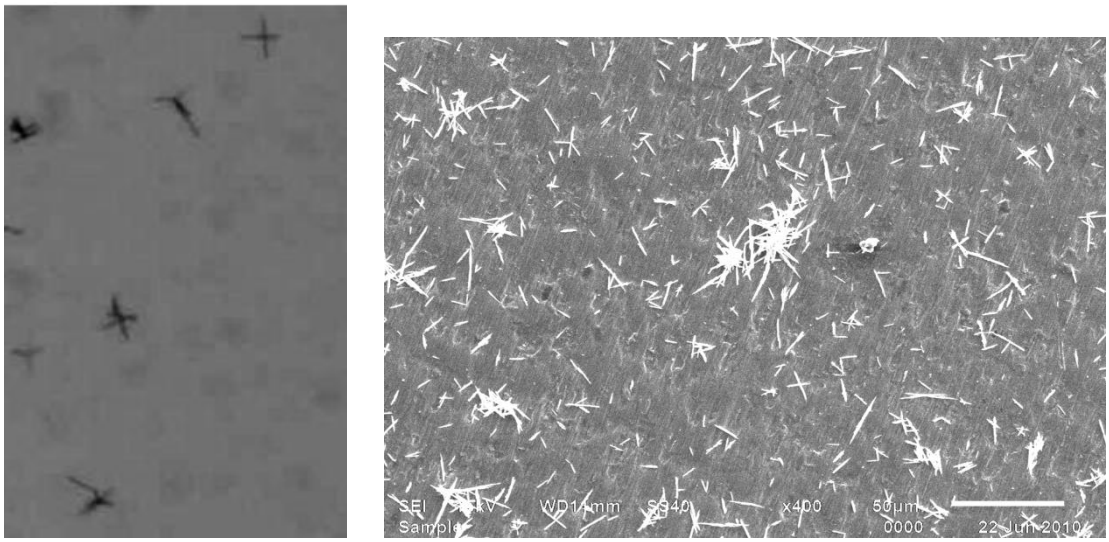

Fig. 4.12 Sample Se B1 a) 33 µm X 66 µm Optical microscope image b) 317 µm X 237 µm SEM image

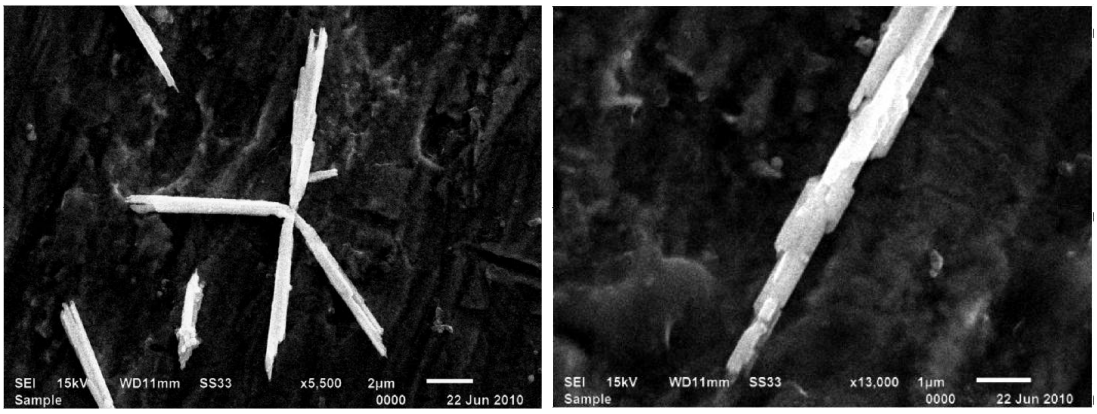

Fig. 4.13 Sample Se B1 SEM images a) 23 µm X 17 µm b) 10 µm X 7.5 µm SEM image

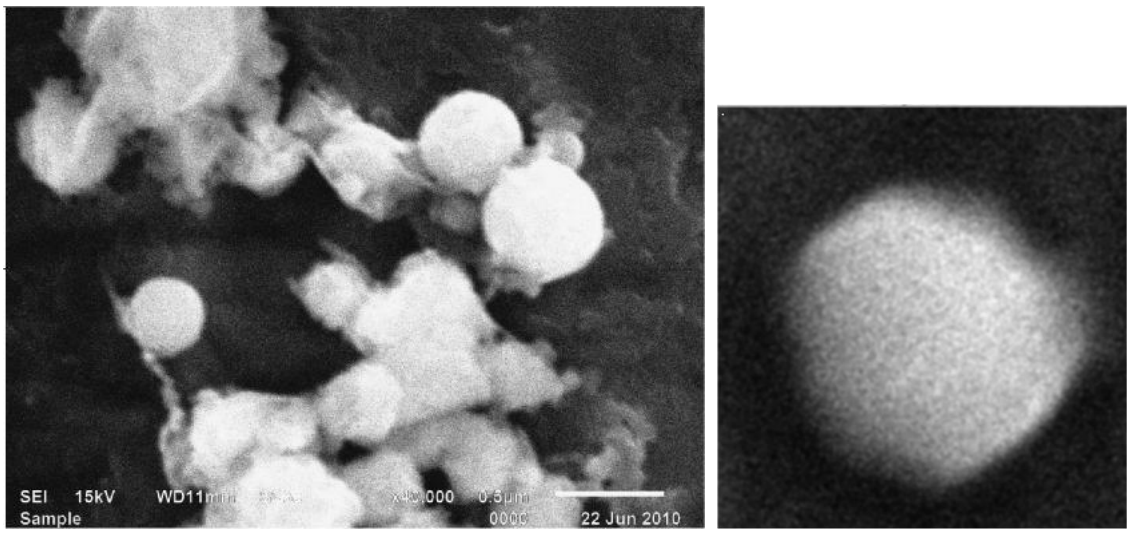

Fig. 4.14 Sample Se B3 SEM images a) 3 µm X 2.5 µm b) 35 nm X 35 nm SEM image

Data analysis:

- The Se B samples are nearly spherical selenium nanostructures interconnected by protein network. (Fig. 4.11)
- Heating at 121 ^{0}C results no change in size and shape. (Fig. 4.14)
- Washing with acetone dissolves the protein and the amorphous nanostructures grow into crystalline asters which show crystalline facets. (Fig. 4.13)
- These asters can actually grow to macro sizes. (Fig. 4.9)

CHAPTER 5

Conclusions

5.1 Conclusions

The aim of the present work was to completely characterize the selenium nanostructures formed via the aerobic microbial route. The Se nanostructures were characterized structurally (XRD, SEM, TEM, Optical Microscope) as well as thermally (DTA, TGA). After this study we derived the following conclusions:

- The Se nanostructures produced by the microbe are amorphous, nearly spherical and held together in clusters by a protein coating.
- Removal of the protein coating by washing with acetone results in growth of crystalline nanostructures. These nanostructures are either rod like with crystalline facets clearly visible or asters. These structures can grow to micron size in length.
- Another method for inducing crystallization is temperature. Heating to ~100 ^{0}C (either in oven or in an autoclave) results in formation of crystalline phase. The nanostructure morphology stays the same.
- The crystalline phase formed in both the routes is hexagonal and the unit cell dimensions are: a = 4.462 A^0, c = 4.980 A^0.
- These results imply that the Se nanostructures produced by the microbe are actually clusters of Se atoms held together in a metastable state by a protein coat. This metastable state can be destroyed either by removing the protein coating or by heat treatment which retains the protein coat and hence the shape, but provides enough energy to the atoms within the cluster to crystallize.

5.2 SCOPE FOR FUTURE WORK

This work can be further extended to characterize the electronic band structure of the various nanostructures (amorphous as well as crystalline) by UV-Vis Spectroscopy and Photoluminescence. The effect of relative concentration of acetone and the biological Se nanoclusters on the morphology of the final structures produced needs further study. This work also has scope to be extended to produce CdSe nanostructures from the Se nanostructures.

CHAPTER 6

References

References:

1. www.mineralszone.com/minerals/selenium.html
2. www.speclab.com/elements/selenium.htm
3. www.statemaster.com/encyclopedia/Selenium
4. http://environmentalchemistry.com/yogi/periodic/Se.html
5. www.chemicool.com/elements/selenium.html
6. http://en.wikipedia.org/wiki/
7. www.gitam.edu/eresource/nano/NANOTECHNOLOGY
8. www.ringsurf.com/online/2003-structures.html
9. www.answers.com/topic/potential-well
10. www.nanocap.eu/Flex/Site/Page.aspx?PageID=4760
11. www.biologyjunction.com/cell_size.htm
12. www.igcar.ernet.in/benchmark/science/43-sci.pdf
13. N.G. Semaltianos et al, EPL Journal, **84**, 2008
14. www.che.ncku.edu.tw/Documents/Publications/Faculty_Intro/Dong-Hwang Chen.pdf
15. Chen Tieshi et al, CJI journal, **11,** No.3, 2009
16. Ming Zhu LIU et al, Chinese Chemical Letters, **15**, No.10, 1249, 2004
17. B. Gates et al, Adv. Funct. Mater, **12**, No.3, 219, 2002
18. N.SAFFUDIN et al, E-Journal of chemistry, **6(1**), 61, 2009
19. http://dspace.mit.edu/bitstream/handle/1721.1/35868/CPE001.pdf?sequence=1
20. Juan ZHANG et al, Chinese Chemical letters, **15**, No 11, 1345, 2004
21. Ronald S. Oremland et al, American society for microbiology,**70,** No 1,2003
22. N. Tejo Prakash et al, Biotechnol Lett, **31**, 1857, 2009
23. Vinod Yadav, M.Sc Thesis submitted in Department of Biotechnology & Environmental Sciences, Thapar University Patiala, 2007
24. http://serc.carleton.edu/research_education/geochemsheets/techniques
25. http://prism.mit.edu/xray/BasicsofXRD.ppt
26. www.mf.mpg.de/de/abteilungen/mittemeijer/english/commentary/Powder Diffraction in Mat.Sci.pdf
27. B.D.Cullity, Elements of x-ray diffraction, 1956, Addison Wesley Publishing Company, Inc.
28. Charles Kittel, Introduction to Solid State Physics, 2007, Wiley India
29. www.mtse.unt.edu/.../3Lecture 6 Optical Microscopy B Compatibility Mod D.p...

30. Vanha.physics.utu.fi/opiskelu/kurssit/…/3-optical microscopy
31. web.utk.edu/~prack/MSE 300/Lightmicroscopyhandout.pdf
32. http://web.utk.edu/~prack/MSE 300/SEM.pdf
33. www.fen.bilkent.edu.tr/~aykutlu/msn/hw/Microscopy.pdf
34. airlab.wkhc.ac.kr/tt/board/ttboard.cgi?act=download&db=histec..
35. www.gitam.edu/eresource/nano/NANOTECHNOLOGY/types_of_electron_microscopy.htm
36. Kaufmann, Characterization of Materials, 2003, Wiley Inter Science, USA
37. www.anorg.chem.uu.nl/.../home.htm
38. http://www.gitam.edu/eresource/nano/NANOTECHNOLOGY/tem.htm
39. http://www.unl.edu/CMRAcfem/temoptic.htm
40. personal.cityu.edu.hk/~bhtan/Thermal.PPT
41. www.iupac.org/publications/analytical_compendium/Cha05sec2.pdf
42. Gottfried W. Ehrenstein et al, thermal analysis of plastics, 2004, Hanser
43. .www.simex.com.mx/PDFS/.../Thermal Gravimetric Analysis brochure.pdf
44. Selenium metal powder, Himedia RM, 2433
45. Sodium selenite (anhydrous), LOBA Chemie, Art 5997
46. Bovine Albumin fraction –V, Himedia RM, 105-5G
47. L-Ascorbic acid (extrapure AR), Sisco research laboratories Pvt. Ltd., 0149100
48. Sodium Dodecyl Sulphate, Sigma-Aldrich, L6026-250G
49. Acetone GR, Merck
50. Paul Cherin et al, **6**, No 8, 1589, 1967